

Published in final edited form as:

*Neuroimage*. 2014 May 15; 92: 120–131. doi:10.1016/j.neuroimage.2014.02.013.

## Modulatory role of the prefrontal generator within the auditory M50 network

Sanja Josef Golubic<sup>1</sup>, Cheryl J. Aine<sup>2</sup>, Julia M. Stephen<sup>3</sup>, John C. Adair<sup>4</sup>, Janice E. Knoefel<sup>5</sup>, and Selma Supek<sup>1</sup>

<sup>1</sup>Department of Physics, Faculty of Science, University of Zagreb, Croatia

<sup>2</sup>Department of Radiology, UNM School of Medicine, Albuquerque, NM 87131, USA

<sup>3</sup>The Mind Research Network, Albuquerque, NM 87106, USA

<sup>4</sup>Department of Neurology, UNM School of Medicine, Albuquerque, NM 87131, USA

<sup>5</sup>Department of Internal Medicine, UNM School of Medicine, Albuquerque, NM 87131, USA

### Abstract

The amplitude variability of the M50 component of neuromagnetic responses is commonly used to explore the brain's ability to modulate its response to incoming repetitive or novel auditory stimuli, a process conceptualized as a gating mechanism. The goal of this study was to identify the spatial and temporal characteristics of the cortical sources underlying the M50 network evoked by tones in a passive oddball paradigm. Twenty elderly subjects [10 patients diagnosed with mild cognitive impairment (MCI) or probable Alzheimer disease (AD) and 10 age-matched controls] were examined using magnetoencephalographic (MEG) recordings and the multi-dipole Calibrated Start Spatio-Temporal (CSST) source localization method. We identified three cortical regions underlying the M50 network: prefrontal cortex (PF) in addition to bilateral activation of the superior temporal gyrus (STG). The cortical dynamics of the PF source within the 30–100 ms post-stimulus interval was characterized and was found to be comprised of two subcomponents, Mb1c and Mb2c. The PF source was localized for 10/10 healthy subjects, whereas 9/10 MCI/AD patients were lacking the PF source for both tone conditions. The selective activation of the PF source in healthy controls along with inactivation of the PF region for MCI/AD patients, enabled us to examine the dynamics of this network of activity when it was functional and dysfunctional, respectively. We found significantly enhanced activity of the STG sources in response to both tone conditions for all subjects who lacked a PF source. The reported results provide novel insights into the topology and neurodynamics of the M50 auditory network, which suggest an inhibitory role of the PF source that normally suppresses activity of the STG sources.

---

© 2014 Elsevier Inc. All rights reserved.

Corresponding author: Selma Supek, Department of Physics, Faculty of Science, University of Zagreb, Bijenicka cesta 32, 10000 Zagreb, Croatia, Tel: +38514605569, Fax: +38514680336, selma@phy.hr.

**Publisher's Disclaimer:** This is a PDF file of an unedited manuscript that has been accepted for publication. As a service to our customers we are providing this early version of the manuscript. The manuscript will undergo copyediting, typesetting, and review of the resulting proof before it is published in its final citable form. Please note that during the production process errors may be discovered which could affect the content, and all legal disclaimers that apply to the journal pertain.

## Keywords

magnetoencephalography (MEG); M50 complex; auditory oddball paradigm; auditory gating; prefrontal inhibition; Alzheimer's disease (AD)

---

## 1. Introduction

The M50, the magnetic counterpart of the P50 event-related potential, is a middle latency component of the evoked neuromagnetic response elicited 40–85 ms after the presentation of an auditory sensory stimulus. The P50 component is also known as the Pb complex, comprised of two subcomponents, Pb1 peaking at about 53 ms and a consecutive Pb2 peaking at about 75 ms post-stimulus (Yvert et al., 2001). The P50/M50 complex is modulated by recency of previous auditory stimuli, thereby providing a measure of the neural ability to modulate its sensitivity to subsequent stimuli (Boutros et al., 1995). Habituation of the amplitude of the P50/M50 complex to redundant input is known as a gating out phenomenon while an increase in amplitude to novel stimuli reflects a gating in process (Boutros et al., 1995). It is assumed that sensory gating predominantly reflects a pre-attentive, automatic (Freedman et al., 1996) filter mechanism that protects the integrity of the higher cognitive centers (Wan et al., 2008). Although dysfunction of sensory gating has been associated with pathophysiology of numerous psychiatric and neurological diseases such as schizophrenia (Adler et al., 1982; Freedman et al., 1996), depression (Garcia-Rill et al., 2002), Alzheimer's Disease (Cheng et al., 2012; Thomas et al., 2010), Parkinson's Disease (Teo et al., 1997) or Huntington's Disease (Uc et al., 2003), effects of aging on the source dynamics of this early activity (40–50 ms post-stimulus) have also been reported (e.g., Aine et al. 2005; Kovacevic et al., 2005; Stephen et al., 2006). To understand the modulation demonstrated by sensory gating requires detailed spatio-temporal analysis of the P50/M50 cortical network to identify inter-subject variability in cortical generators and their individual dynamics when this network is functioning optimally and when it is not. We used noninvasive MEG recordings with high temporal and spatial resolution not only to identify the M50 cortical network but also to address the basic mechanism underlying sensory gating modulations.

Although numerous studies have explored the modulation of the auditory P50/M50 components and suggested multiple generators, there is no agreement on the underlying network. The temporal dynamics of the cortical sources active during the early and middle latency interval (i.e. the morphology of the cortical response during 30 - 100 ms post-stimulus) were reported rarely and only for the sources localized in the superior temporal gyrus (STG) (Huang et al., 2003; Thoma et al., 2003). The STG origin of the middle-latency auditory evoked response is suggested by scalp distribution of electrical potentials (Cacace et al., 1990; Edgar et al., 2003; Reite et al., 1988; Yvert et al., 2001), confirmed by intracranial recordings (Liegeois-Chauvel et al., 1994), and has been further verified by MEG recordings (Thoma et al., 2003; Lu et al., 2007; Yvert et al., 2001). However, MEG measurements have indicated that along with the expected bilateral sources in the area of the superior temporal lobe there is at least one additional generator that contributes to the P50/M50 auditory response (Huotilainen et al., 1998; Reite et al., 1988). The key finding

supporting the existence of additional generators was the presence of the auditory P50 component after bilateral temporal lobe lesions (Woods et al., 1984). Invasive animal studies have suggested a hippocampal source as an additional contributor to the P50 complex (Freedman et al., 1996), while intracranial depth electrode recordings in epileptic patients found no evidence of hippocampal involvement in the generation of the P50 potential (Grunwald et al., 2003). Later intracranial measurements revealed the main generators of the P50 in the temporal lobes with substantial contribution from frontal lobe activity in half of the epileptic patients studied (Korzyukova et al., 2007). Recent MEG studies using current density reconstruction for spatial localization of the M50 generators affirm the contribution of frontal cortex activity to the extracranial M50 response, but without agreement on the temporal lobe contribution (Garcia-Rill et al., 2008; Weiland et al., 2008).

Auditory P50/M50 components are usually examined using an oddball paradigm, paired click paradigm or short trains of auditory stimuli. Patients with Alzheimer's disease (AD) demonstrate a deficiency in suppressing the evoked P50/M50 auditory response to the second click of paired click stimuli (Cancelli et al., 2006; Jessen et al., 2001; Thomas et al., 2010) and the standard tones of an active or passive oddball paradigm (Cheng et al., 2012; Golob et al., 2009). Furthermore, AD patients manifest a significant decrease in cortical thickness of the lateral temporal and inferior frontal regions (Lerch et al., 2008), in addition to pathophysiological attributes of disease found in the hippocampus, entorhinal and anterior frontal cortex (Price et al., 1991). Observed deficits of auditory gating in AD patients may reflect a change in the number or spatial location of cortical sources that comprise the M50 component and/or an alteration of their activity. Given that major neurodegenerative changes associated with AD are found in the frontal and temporal lobes, which are assumed to be the main generators of the M50 auditory component, changes in the number and dynamics of the generators in this population, compared to healthy controls, should allow the differential examination of their individual roles.

MEG offers both high spatial and high temporal resolution, which are fundamental to the study of the topology and cortical source dynamics underlying auditory evoked brain responses. Advanced approaches in MEG multi-source modeling techniques and high-channel density whole-head systems have the potential to offer non-invasive, novel insights into the M50 neural generators. In this study we utilized a 275 channel whole-head system for MEG measurements together with a multi-dipole Calibrated Start Spatio-Temporal (CSST) localization technique (Ranken et al., 2002; 2004) to: a) identify the topology and dynamics of the M50 cortical networks evoked by tones in a passive auditory oddball paradigm in healthy elderly subjects and patients with MCI and probable AD; and b) compare this network of activity in healthy versus disease states to acquire more information about the function of this network. We opted for an auditory oddball paradigm because it enhances the activation of frontal areas. In contrast, prefrontal activity may be attenuated during a paired click paradigm. Paired click stimulation, which has a constant probability of a repeating long-term pattern (S1 ~500ms S2 ~8s), may cause long term suppression of prefrontal (PF) activity since PF cortex is presumed to function as a mediator of high-level executive functions that enhances goal-directed activations on a longer temporal scale (Shimamura, 2000). A recent study showed that both behavioral and neural priming (response reduction) can also exhibit response or decision specificity (Dobbins et al., 2004).

A passive oddball paradigm, which was employed in this study, evokes an automatic response to both tones of the paradigm and it does not require any behavioral response that might obscure basic sensory processing, which is of particular importance for elderly and demented subjects.

## 2. Methods

### 2.1 Subjects

Twenty right-handed elderly participants (5 females) ranging from 63 to 83 years of age (mean = 74 years) participated in the study. Ten of the participants, diagnosed as either amnesic mild cognitive impairment (aMCI) or probable AD were recruited from the memory disorders clinic at the New Mexico Veterans Health Care System. AD patients satisfied DSM-IV and NINCDS-ADRDA criteria for probable AD diagnosis. The participants in the MCI group showed mild memory decline which did not impede routine activities of daily living and they were not demented according to DSMIV (criteria modified from Petersen 2004). Healthy elderly participants were recruited from the community (>65 years, mean = 73 years) with self-reported normal cognitive ability. All participants underwent a screening evaluation including a quantitative neurological examination, the Physical Self-Maintenance Scale, the MiniMental State Exam (MMSE), the Geriatric Depression Scale, structural brain magnetic resonance imaging (MRI), and a modified Hachinski Ischemic Scale to exclude other causes of cognitive impairment. Exclusion criteria included history of psychiatric illness including psychosis and major depression, and other medical conditions (e.g., Chronic Obstructive Pulmonary Disease, Coronary Heart Disease, epilepsy, Parkinson's disease) as well as alcohol or substance abuse. Written informed consent was obtained from all participants according to the 1964 Declaration of Helsinki. This research was approved by the Human Research Review Committee at the University of New Mexico, Health Sciences Center and by the Research and Development Committee at the New Mexico VA Health Care System.

### 2.2 MEG data acquisition

MEG data were acquired with a CTF 275-channel whole-head system (VSM MedTech, Ltd.) inside a magnetically shielded room at the Mind Research Network in Albuquerque, New Mexico. Participants were seated comfortably in a chair with the head centered within the measurement helmet. Neuromagnetic activity was continuously recorded with a sampling rate of 600 Hz with online filters at 0.1 to 200 Hz. For eye blink artifact identification and elimination, EOG signals were simultaneously recorded with the MEG signals. Electrodes were placed below the right eye and above the left eye for eye blink or eye movement stronger than 75  $\mu$ V. A 3-D digitizer (Polhemus) registered the subject's nasion and the left and right preauricular points for establishing the 3-D coordinate head frame, as well as additional points along the surface of the head for later co-registration with structural MR images. For each subject anatomical T1-weighted MPRAGE (1.5 mm slices) and T2 weighted Turbo Spin Echo (1.8 mm slices) magnetic resonance images were obtained from a 1.5-T Siemens Sonata MR scanner at the Mind Research Network. The tones of the oddball paradigm were presented using NBS Presentation software and were delivered inside the magnetically shielded room to the participant's ear canal using Etymotic

Research ER-3A sound transducers with plastic tubing. A passive auditory oddball task consisted of 500 binaurally presented tones of which 80% (400 trials) were standards (1000 Hz) and 20% (100 trials) were deviant (1200 Hz) tones. Tone duration was 200 ms. The inter-stimulus interval was 1000 ms on average with a jitter range of 200 ms. Adjustments in the intensity of the tones were made for each participant separately, based on the results of a hearing threshold test performed with the ear-inserts in place while in the shielded room in order to achieve a level of 60dB SPL.

### 2.3 Data processing and filtering

The data were pre-processed using CTF software for deletion of large amplitude single-epoch MEG responses (which exceeded a threshold of 3pT/cm) and offline averaging (filtered at 0.1 to 50 Hz). MEGAN (MEG ANalysis), an MEG data visualization and analysis tool developed by Elaine Best, in the Biophysics group, Los Alamos National Laboratory, was used to remove baseline noise (estimated from the -100 to 0 ms pre-stimulus interval) and for producing and displaying NetMEG files for later processing. MRVIEW software (Ranken et al., 2002), used for further processing, includes: 1) semi-automated segmentation of volumetric head data; 2) an interactive coordinate alignment method (to integrate volumetric MRI head data with MEG data) which utilizes surface visualization; 3) MEG/EEG forward simulator; and 4) a Calibrated Start Spatio-Temporal (CSST) tool (Ranken et al., 2002) for multi-start, multi-dipole MEG spatio-temporal source localization. For more details on these procedures and in-depth testing of the CSST analysis algorithm please see Aine et al. (2010, 2012) and Sanfratello et al. (in press).

### 2.4 Multi-dipole, spatio-temporal modeling

Cortical sources of the auditory evoked fields (AEF) (both empirical and simulated), were modeled by multiple current dipoles. A segmentation procedure was used to segment the cortical surface from the high-resolution MRI data. 3D morphological operations were applied to obtain a layer of voxels that approximate the gray/white matter boundary. The best-fitting sphere for the head model was estimated from the segmented cortical surface. Spatio-temporal source analysis of data acquired from all channels was conducted using the multi-dipole CSST algorithm (Ranken et al., 2004) which uses a semi-automated multi-start downhill simplex search for determining the locations, strengths and orientations (Aine et al., 2000; Huang et al. 1998) of activated cortical foci. Estimation of the time invariant parameters (locations, orientations) was derived first using nonlinear minimization, followed by a linear estimation of the associated time varying parameters (source strengths). Starting points for each model, needed for simplex calculations, were randomly selected from the segmented cortical surface and from a moderate number of additional MR-derived locations within the brain volume. This approach reduces the possibility of biasing the results toward previously reported areas of activity. In our calculations, starting points were selected multiple times to initiate the fitting procedure. Depending on the model order assumed, up to 12,000 starting points were used for empirical and up to 4,000 for simulated data. Spatio-temporal source localization was conducted within both 30–100 ms and 30–200 ms post-stimulus time windows as a check on the internal consistency of the identified cortical network underlying the M50 complex. The best fitting parameters were obtained by minimizing the reduced  $\chi^2$  value (Supek and Aine, 1997). The minimum number of dipoles

was estimated using singular value decomposition (SVD) of the spatiotemporal matrix in the selected time interval. Selection of the adequate model was based on: 1) the reduced chi-square measure of goodness-of-fit; 2) proportion of variance explained (PVE) value; 3) dipole clustering across multiple fits to assess location scatter (an indication of over-modeling, Supek and Aine, 1993); 4) the residual waveforms to assess whether additional signal remained (an indication of undermodeling); and 5) the inspection of source time-courses (near-zero amplitude across the entire time interval is an indication of over-modeling). The 10 best fitting solutions from every inverse calculation were saved for further viewing and analysis. Estimation of confidence regions for the best-fitting dipole solutions were obtained by Monte Carlo simulations using the source locations from the best-fitting model as starting locations in the minimization procedure (Medvick et al., 1989). To provide an estimate of the effect of noise, 100 simulations were conducted by adding noise based on the pre-stimulus (–100 to 0 ms) noise level determined by the sensor baseline noise variance.

## 2.5 Anatomical locations

Anatomical locations of the dipoles were assessed by aligning the MEG head-centered coordinate system with participants' MRI head-centered coordinate system. The coordinate system corresponded to the following convention: the positive x-axis points toward the nose, the positive y-axis points towards left ear and the positive z-axis points out the top of the head. The criterion for selecting STG sources was its localization within 1 cm of Heschl's gyrus and not above the Sylvian fissure while localization within frontopolar (BA 10) and orbitofrontal (BA 11) portion of prefrontal cortex was the criterion for the PF source relative to each individual participant's MRI.

## 2.6 Statistical analyses

Cortical locations and time course estimates were examined for each source and each subject, for the two conditions (standard and deviant) and two time windows (30–100 ms and 30–200 ms). First, data sets were tested for the basic assumptions underlying analysis of variance (ANOVA): normality of distribution and homogeneity of variances. The Kolmogorov - Smirnov test was carried out to verify the normality of distribution and Bartlettov - Box test was used to check homoscedasticity of variance. Post-hoc comparisons were conducted using Tukey's Honestly Significant Difference (HSD) test to isolate interaction effects. Repeated measures (RM) ANOVA was conducted on the estimated model order (number of localized dipoles), amplitudes and maximum peak latencies of their estimated cortical dynamics in the 30–100 ms time windows across participants. The factors submitted to ANOVAs consisted of: hemisphere (dynamics of Left and Right STG source in each subject), condition (Standard and Deviant tones) and network type (with and without PF activation). Additionally, in order to exclude influences of source depth and individual cortical geometry (source orientations) on amplitude of estimated peaks, ANOVA was performed on the relative amplitudes of the first two peaks (Mb1 and Mb2) to the amplitude of the most prominent response (M100) identified in estimated time courses of STG sources within the 30–200 ms time window.

## 2.7 Numerical simulations

Numerical simulations were carried out using the forward simulator within MRIVIEW to verify the sensitivity and robustness of our CSST algorithm for localization of a low-amplitude PF source that is simultaneously active with strong bilateral activity of the STG regions (putative primary auditory cortex). A limited set of simulations was conducted assuming point current dipole generators located bilaterally in the superior temporal gyri (STG) and PF cortex (orbitofrontal position). Simulated neuromagnetic field distributions were generated assuming a 275-channel CTF sensor configuration and a spherical head model. The simulated current dipolar sources consisted of three focal patches (1 voxel each) placed within a realistic MRI-derived geometry of participant S2. Two sources were placed in the vicinity of the STG, one in each hemisphere, and the third was placed in prefrontal cortex. STG sources were placed superficially (at a depth of 0.9 cm) while the PF source was placed at a depth of 3.24 cm from the cortical surface. Temporal dynamics of the dipoles were designed to exhibit activity analogous to the corresponding source dynamics estimated from the evoked auditory responses during 30–100 ms time interval. Time courses were modeled using Gaussians to form two peaks for the two STG and the PF time courses. The amplitude of the first STG peak was set at 15 nAm with a standard deviation of 4 ms (full width at half maximum on the t-axis) while the second STG peak was set at 40 nAm with a standard deviation of 7ms. The mean latencies for the STG peaks were slightly different for the right (51 ms and 78 ms) and the left (55 ms and 83 ms) Gaussians. A series of noisy field distributions were calculated assuming three source configurations of fixed locations (two STG and one PF source), fixed time courses of the two strong STG sources, and time courses of the weaker PF source that varied. The following peak amplitudes of the Mb1c and Mb2c peaks were used for simulating a series of time courses of the attenuated PF activity: 9 nAm and 15 nAm; 6 nAm and 10 nAm; 4.2 nAm and 7 nAm; 3 nAm and 5 nAm; 2.4nAm and 5nAm; and 2.4 nAm and 4 nAm, respectively. The mean latencies of the PF peaks (i.e. 48 ms for the first and 73 ms for the second) were kept constant while PF source strength was systematically attenuated. In addition to simulating noisy field distributions by adding empirical noise from the pre-stimulus interval (–100 - 0 ms), empirical noise at 125% amplitude of the baseline noise level from the same interval was also added to forward solutions to simulate extreme conditions of a very low SNR that was expected to adversely affect the ability to localize PF source activity. Source localization was conducted using two and three dipole models for the noisy simulated forward fields. For each of the source location estimates in the three-dipole model, the Euclidian distance from the estimated to the given location of the dipole was calculated as a measure of the location bias.

## 3. Results

### 3.1 Cortical generators of the M50 complex

**3.1.1. Auditory evoked field responses**—Visual inspection of the auditory evoked field responses revealed two prominent peaks in the 30–100 ms post-stimulus time window for all participants: the first peak was evident at 40–55 ms and the second peak appeared 70–89 ms post stimulus for both tones of the oddball paradigm (Fig.1). These auditory evoked field (AEF) components, labeled as Mb1 and Mb2, represent a magnetic counterpart of the M50 complex, and correspond to Pb1 and Pb2 peak components of the human auditory

potentials, referred to as the P50 (Pb) complex (e.g., Yvert 2001). Detailed visual inspection of the individual sensory responses identified the strongest Mb1 and Mb2 peaks of the evoked activity recorded at temporal sensors over both hemispheres (from MLT/MRT11 to MLT/MRT57) in all subjects in both conditions. Weaker but detectable M50 activity was recorded at frontal sensors (from MLF11 to MLF67) for 10/10 healthy subjects. AEF responses evoked by deviant tones were generally stronger during the entire recording time for all participants.

**3.1.2 Spatial localization**—To identify M50 generators, the multi-dipole spatio-temporal localization of AEF data was conducted in the 30–100 ms post-stimulus time window for both tone conditions. The CSST localization approach identified 2–3 cortical sources during the selected interval across participants and across conditions. Panel A) of Fig.2 shows three brain regions underlying the M50 for the standard tone: bilateral STG activity and the PF region. The STG activity was localized in 20/20 participants for both tone conditions (bilateral in 18/20). A PF source was localized in all 10 healthy subjects (10/10) for the deviant stimulus and 4/10 for the standard. PF sources were localized to orbitofrontal (ventromedial surface of the frontal lobe; BA 11) or medial parts of anterior prefrontal cortex (BA 10) across subjects ( $x = (5.58 \pm 0.71)$  cm;  $y = (-0.15 \pm 0.38)$  cm;  $z = (2.64 \pm 0.68)$  cm in MRI head-centered coordinate system). There were no significant within-subject differences in the spatial locations of the identified sources evoked by the two stimulus conditions (RM ANOVA, main effect of condition; PF:  $F(1,13) = 0.23$ ,  $p = 0.64$ ; left STG:  $F(1, 34) = 0.11$ ,  $p = 0.75$ ; right STG:  $F(1, 38) = 0.11$ ,  $p = 0.65$ ). The PF source was not localized for either tone in (9/10) subjects from the patient group. Post-hoc power analyses based on the sample size and observed very large effect size ( $r_\phi = 0.904$ ), demonstrated very high statistical power (100%) and specificity (90%) of our localization results.

**3.1.2 Stability of localization**—To confirm the stability of the localization results, spatio-temporal localization was also conducted also within the 30–200 ms time window. Panel B of Fig.2 shows the four dipole configuration localized from the 30–200 ms window which reveals three sources were also localized in the 30–100 ms interval (panel A). An additional region (red dot in the panel B) was active in the right anterior temporal region. Localization results in Fig. 2 were obtained for the same participant and the same tone condition. Generally, 2–5 sources were identified during the 30–200 ms time window which supported the localization results obtained from 30–100 ms time interval across subjects. Additional sources found in the longer time interval were located in parietal and/or anterior temporal regions. There was no statistically significant difference in the number of localized dipoles due to condition, i.e., standard vs. deviant tone (RM ANOVA,  $F(1,2,38) = 0.19$ ,  $p = 0.69$ ). Monte Carlo simulations (not shown) demonstrated that realistic measurement noise would result in localization scatter of only a few millimeters (up to 6 mm) for all identified sources across participants, for both conditions.

**3.1.3 Reliability of localization**—Fig. 3, panel A, represents AEF recordings during the 30–100 ms time window acquired from the frontal sensors (from MLF11 to MLF64) for two representative subjects (S2 and S3). The peaks of the AEF responses are evident only in the waveforms of subject S2. They are diminished in the waveforms of subject S3 and were

comparable to the noise level. The corresponding iso-field contour maps of the neuromagnetic field distributions evoked by the standard tone at selected latencies are displayed for both subjects in panel B for the Mb2 component. The formation of a dipolar field pattern in the frontal regions for subject S2 is evident in the time intervals corresponding to Mb1 (not shown) and Mb2 field component, while the equivalent maps of subject S3 lack any dipolar-like field pattern. Panel C displays the results of the spatio-temporal modeling of the complete data set, not just the frontal sensors' data shown in this figure, which localized PF and bilateral STG sources underlying the M50 complex for subject S2. Only bilateral STG sources were localized for subject S3.

**3.1.4 Sensitivity of localization: Numerical simulation**—Fig. 4 shows the results of numerical simulations conducted to explore the sensitivity of our approach to identify a low amplitude frontal source simultaneously active with high amplitude STG sources. While the maximal strength of STG sources was kept high and constant (40 nAm), the frontal source strength was systematically attenuated from 15 nAm downwards. CSST source localizations were conducted by applying 2- and 3-dipole models to a series of simulated noisy data. Panels A and B of Fig. 4 show the simulated 3-source configuration together with modeling results for two noise conditions representing extreme cases of the series of simulated PF dynamics: a relatively strong PF source (Mb1c and Mb2c peak amplitudes of 9 nAm and 15 nAm, respectively) and a very weak PF source of only 2.4 nAm (Mb1c) and 5 nAm (Mb2c).

Two-dipole solutions had considerably lower reduced  $\chi^2$  ( $<1$ ) and PVE values for all conditions (not only the two shown in Fig. 4) compared to the adequate three-dipole model related to high noise conditions. However, even in the highest noise condition (125% of empirical noise) the maximal source strength of only 5 nAm (Mb2c peak amplitude) at a depth of 3.24 cm was of sufficient strength that CSST localized a frontal source in the presence of even 8 times stronger, synchronously active superficial bilateral STG sources (panel B). High levels of added noise had a stronger influence on the source dynamics than on the spatial location of the estimated sources.

Table 1 presents PF source strength-related localization errors for noisy 3-dipole modeling of simulated data generated assuming a realistic MRI-derived cortical surface of subject S2. The localization error for the frontal source was inversely proportional to the maximal dipole strength but the overall error was less than 1 cm for all noisy 3-dipole estimates. A spatial bias less than 0.4 cm was found for STG sources from the 3-dipole models (Table 1), while a 2-dipole model localized sources relatively close but slightly rostral from the actual locations of the STG sources (Fig. 1, panel B).

### 3.2 Cortical dynamics of the STG generators underlying the M50 complex

The Kolmogorov - Smirnov method showed that none of the data distributions (amplitudes and peak latencies of the evoked cortical activity underlying the M50 complex) were significantly different from a normal distribution. STG sources were localized bilaterally in most subjects (18/20) without systematic differences between the hemisphere activations (RM ANOVA, main effect of hemisphere; latencies, amplitudes,  $p > 0.05$ ), hence the STG time courses were averaged across hemispheres for each individual. Fig. 5 reveals two

identifiable peaks of the STG activation in the 30–100 ms time window: an early peak (at 35–53 ms range latency across subjects; 19/20) and a late peak (at 75–99 ms range latency across subjects; 20/20) for both tone conditions. To distinguish between localized cortical sources from response components described at the sensor level (Mb1 and Mb2), we labeled the peaks of cortical components as Mb1c and Mb2c. Amplitude differences of Mb1c and Mb2c peaks in the STG responses across conditions are evident in Fig. 5. The comparison between tone conditions showed significantly stronger amplitudes of Mb1c and Mb2c peaks in the STG responses to the deviant tone across subjects (RM ANOVA, main effect of condition; Mb1c:  $F(1, 38) = 4.65$ ,  $p = 0.04$ ; Mb2c:  $F(1, 38) = 4.77$ ,  $p = 0.03$ ) but there was no significant difference in their latencies as an effect of condition.

### 3.3 Cortical dynamics of the PF generator underlying the M50 complex

In subjects whose PF source was identified, two peaks of the maximum activity in the 30–100 ms time window were found in the time course as shown in Fig. 5. Mb1c and Mb2c components in the PF source, evoked by standard stimuli, appeared at 46–50 ms and 80–88 ms post-stimulus, respectively, while the maximum activity evoked by deviant tones occurred at 40–49 ms and 62–78 ms post-stimulus (Fig. 5). Latencies of both peaks, Mb1c and Mb2c, appeared earlier in response to the deviant tone (RM-ANOVA, main effect of the condition; Mb1c:  $F(1, 13) = 7.24$ ,  $p = 0.02$  and Mb2c:  $F(1, 13) = 21.86$ ,  $p < 0.001$ ), but a significant difference in amplitude as an effect of condition was not found (RM-ANOVA, main effect of the condition; Mb1c, Mb2c,  $p > 0.05$ ).

### 3.4. Modulatory role of the PF source on STG dynamics

Statistical analyses performed on individual subjects' peak amplitudes and latencies obtained from the 30–100 ms interval of the STG time courses show significantly lower amplitude (52%) of the Mb2c peak in subjects whose network included PF activation (RM ANOVA; Mb2:  $F(1, 18) = 23.85$ ,  $p < 0.001$ ) evoked by the standard tone. Also, we found significantly lower amplitudes of both STG peaks, Mb1c (43%) and Mb2c (56%), evoked by the deviant tone in subjects with the activated PF source within the M50 network (type 1) compared to subjects without PF activation (type 2) (RM ANOVA; Mb1c:  $F(1, 18) = 7.32$ ,  $p = 0.02$  and Mb2c:  $F(1, 18) = 9.45$ ,  $p = 0.008$ ). Fig. 6 shows mean latencies and amplitudes of both M50 components localized in STG and PF time courses across network types and conditions. To avoid the possible influence of an individual's cortical geometry on the grand averages (according to the network type) of Mb1c and Mb2c peak strength, we first normalized the amplitudes of Mb1c and Mb2c peaks relative to M100c (the most prominent peak within 30–200 ms responses of the STG sources within condition) for each subject across conditions. In addition to this, we conducted statistical analyses across types of the M50 network, i.e. with and without the accompanied PF activation (Fig. 6). ANOVA confirmed a significantly lower averaged relative strength of the Mb2c peak in the presence of frontal activity (0.45 vs. 0.88) evoked by the standard tone (RM ANOVA; Mb2c:  $F(1, 18) = 21.85$ ,  $p = 0.004$ ) and confirmed a significantly lower averaged relative strength of both M50 subcomponents in the presence of frontal activity (0.27 vs. 0.30 for Mb1c and 0.52 vs. 0.79 for Mb2c) evoked by the deviant tone (RM ANOVA; Mb1c:  $F(1, 18) = 5.12$ ,  $p = 0.049$ ; Mb2c:  $F(1, 18) = 8.46$ ,  $p = 0.009$ ). Latencies of both peaks, Mb1c and Mb2c, of the PF source were, in both conditions, and for all subjects, earlier than the respective STG

peaks. The average difference between STG and PF peak latency was  $(1.25 \pm 1.6)$  ms for Mb1c and  $(15.5 \pm 1.8)$  ms for Mb2c peak in the frequent tone condition. In the rare tone condition, the PF components peaked  $(6.1 \pm 3.9)$  ms earlier for Mb1c and  $(14.6 \pm 9.3)$  ms for the Mb2c.

A significant influence of the PF source on latencies of both M50 subcomponents of the STG responses were found to the deviant tone (RM ANOVA; Mb1c,  $p = 0.038$ ; Mb2c,  $p = 0.04$ ) as manifested by earlier STG responses in subjects with the activated PF generator. Standard tone stimulation revealed no significant difference in latencies of the STG subcomponents with respect to subjects with different types of auditory network patterns (with and without the PF activation).

### 3.5 Effect of the stimulus conditions on the M50 network types

To examine the effect of stimulus condition (standard vs. deviant tone) on the M50 network types, subjects were grouped according to the localization of the PF generator, i.e. subjects with a 3-generator M50 network evoked by both tones of the auditory paradigm (bilateral STG and PF) and participants with no PF generator regardless of the tone condition. The STG amplitude of the Mb1c peak of the first group was 30% weaker for the standard than for the deviant tone (Fig. 6). The group of participants lacking the PF source had 50% weaker Mb1c amplitudes evoked by the standard tone compared to the deviant. A comparison of Mb2c peaks in the STG time courses according to the condition revealed 12% weaker amplitudes evoked by the standard than by the deviant tone in the first group, while 19% weaker responses were found for the second group (Fig 6).

## 4. Discussion

This study characterized the spatio-temporal pattern of cortical sources involved in the M50 network evoked by tones in an oddball paradigm. The selective activation of a PF source within the M50 network according to subject category (healthy elderly versus cognitively-impaired elderly) enabled a differential analysis of the functional role of the individual sources within the M50 network. Our multi-dipole, multi-start CSST source localization approach revealed three cortical regions underlying the M50 in healthy elderly: bilateral STG and PF cortex. To our knowledge, this study provides the first estimates of the PF source dynamics during the 30–100 ms time interval, which was found to have two cortical sub-components peaking successively at 46–50 ms (Mb1c) and 80–88 ms (Mb2c) post-stimulus. Depending on subject diagnostic category it was possible to distinguish two types of an early, task-activated auditory network underlying the M50 complex evoked by tones in an oddball paradigm, i.e., with (healthy) and without PF activation (cognitively impaired). Based on the excellent separation of groups related to the presence or absence of PF activation, the network with PF activation is further described as a ‘functional’ network configuration whereas the absence of PF activation is considered as a ‘dysfunctional’ network configuration. Early activation of sources in the STG region, prominent in both network types, varied as a function of the presence or absence of PF activation. The M50 components of the estimated STG dynamics in the absence of PF activity (i.e., dysfunctional network) demonstrated significantly increased amplitude for both tone conditions (standard

and deviant) in comparison with the network type that included the PF source. The PF source peaks were earlier than corresponding STG peaks in all subjects whose network type included PF activation. Our finding of enhanced STG activity in the absence of a PF source together with the earlier PF peak activation suggests an inhibitory role of PF cortex on the bilateral STG sources for both tone conditions. However, this cross-sectional study cannot provide definitive information concerning the direction of causality of observed correlations between the PF and STG sources; therefore, the “modulatory” role of PF remains speculative until further studies can be conducted to determine directionality.

#### 4.1 Spatio-temporal localization of M50 network

The M50 network topology identified in this study is consistent with results of previous P50/M50 studies confirming not only the contribution of putative primary auditory cortex in the superior temporal lobe (Huang et al., 2003) but also activation of an additional source in the prefrontal cortex. While earlier studies suggesting frontal lobe activation (Garcia-Rill et al., 2008; Weiland et al., 2008, Korzyukova et al., 2007) used minimum norm approaches and detected only a diffuse activity within the frontal lobe this is, to our knowledge, the first report of both the localization of the M50 source in the medial PF cortex and characterization of its dynamics. The sensitivity of the MEG signals to changes in depth, cortical extent, cortical morphology and noise level, as well as the use of multi-dipole source modeling have been examined in numerous studies (Aine et al, 2012; Josef Golubic et al., 2011; Ahlfors et al., 2010; Stephen et al. 2003, 2005; Huang et al, 1998; Supek and Aine, 1993, 1997; Mosher et al., 1992,). Numerical simulation results strongly indicate that source depth and its cortical extent are the main factors that compromise the sensitivity of MEG to neural activity in the human cortex (Josef Golubic et al., 2011; Hillebrand and Barnes, 2002). Contrary to a widely accepted assumption, it has been shown that source orientation is not a significant factor in limiting localization (Leahy et al., 1998; Hillebrand and Barnes, 2002). The high sensitivity of MEG sensors to neuromagnetic fields originating in the STG implicates a more superficial, and more tangentially oriented (with respect to the head surface) cortical current moment that is easily detected with MEG, while generators in the PF region, especially in its inferior parts, may have poor detectability due to their distal positions from the sensor array. Since source depth but not source orientation is the major limiting factor for detection probability, the sensitivity of detection can be increased by using extensive sensor coverage around the head. Therefore, the present study used a whole head sensor array composed of 275 axial 1st order gradiometers while synthetic third gradient balancing was used to effectively remove background noise on-line, thereby augmenting detectability of the evoked neuronal activity and enabling the localization of low amplitude frontal generators. For multi-dipole, spatio-temporal source localization we used a semi-automated multi-start downhill simplex algorithm which utilizes thousands of starting points randomly selected from a realistic head geometry. All dipole modeling techniques require starting locations and most require that the starting locations be provided by the user, thereby possibly biasing the source locations that are identified. CSST minimizes bias toward anticipated areas of activity by randomly choosing starting locations from the entire head volume. Using this approach we gained a comparative advantage over previous MEG studies that implemented user-defined starting locations for dipole modeling. Moreover, spatiotemporal source localization provided estimates of the temporal dynamics

of multiple cortical regions in the selected time interval covering the M50 complex that previous studies have not reported.

We demonstrated the reliability and stability of our spatio-temporal modeling during the 30–100 ms time window by: 1) evaluating AEF transient responses and their corresponding iso-field contour maps of the neuromagnetic field distributions from frontal sensors in individual subjects before examining data across subjects (Figs. 1 and 3); 2) applying the localization algorithm to an overlapping 30–200 ms interval to examine internal consistency of the data (Fig. 2); 3) estimating cortical dynamics and identifying Mb1c, Mb2c, and M100 peaks with rather small standard deviations (Fig. 5); and 4) conducting a series of numerical simulations to explore the overall sensitivity for detecting low amplitude PF sources simultaneously active with high amplitude STG sources placed in both hemispheres (Fig. 4). Simulations showed that the maximal dipole strength of 5 nAm at a depth of approximately 3.24 cm was sufficient for a reliable PF source localization. A source strength of 5 nAm, which was the threshold of our spatio-temporal localization approach, is in agreement with results by Hillebrand and Barnes (2002).

Activation of a PF source within the M50 network is anatomically supported by reports of dense bidirectional connections between medial PF and superior temporal cortices in primate and human anatomical studies (Barbas et al., 1999; Croxson et al., 2005). The orbitofrontal cortex (OFC) and medial PF cortices share extensive cortico-cortical connections, including extensive local projections to and from other PF regions, as well as with motor, limbic, and sensory cortices (Cavada et al., 2000). The structural properties of the connecting pathways provide the means for localized STG and PF regions to work together as a large-scale neural network.

Beyond neurobiological plausibility of connections between orbitofrontal regions and STG cortex, diverse functional studies have also identified activations in OFC, suggesting that this prefrontal field is a component of brain networks critically engaged in memory, expectation, sensory integration (Kringelbach, 2005) and participates in the executive control of information processing by inhibiting neural activity associated with irrelevant or uncomfortable (e.g. painful) stimuli (Shimamura, 2000). Studies suggest that “top-down” inhibitory control mechanisms originate from OFC (Knight et al., 1989). Furthermore, patients with OFC lesions revealed a P300 neural response that did not habituate over successive trials with enhanced activity recorded at frontal electrodes (Fz) 150 ms after a somatosensory stimulus was delivered (Rule et al., 2002). These data suggest that the OFC normally inhibits aversive sensations early in sensory processing by regulating neural activity in sensory association areas. Our MEG results provide support for such a model and suggest (10/10 healthy subjects) a role for a medial PF generator even in very early sensory processing. The data permitted us to develop a testable model of how prefrontal activity inhibits STG activity that can be evaluated in future studies.

However, localization of an additional PF source in the M50 network may be related to compensatory processes often suggested in aging studies (i.e., an additional source(s) is invoked in elders to compensate for the degradation of a network(s) due to age) or it may result from the employment of different strategies reported previously with increasing age

(Aine et al., 2006; 2011; 2014; Cabeza et al., 2002; Logan et al., 2002). For example, Aine et al. (2005) revealed PF activation in elderly subjects twice as often as in younger participants in an auditory incidental learning paradigm. Although, this study examined responses to repetitive stimulation (words), it required higher-order cognitive processing than simply listening to tones and thus, it is conceivable that strategy differences between the young and old may have played a role in this study. The oddball paradigm, in contrast, evokes more sensory-related processes. The responses evoked by an oddball paradigm also permit one to examine the effects of novel input (gating in) as well as inhibition induced by repetitive stimuli (gating out) (Boutros et al., 1995; Ermutlu et al., 2007). Consequently, the M50 responses evoked by the oddball paradigm may invoke complex sensory processes, different from that evoked with a paired-click paradigm, but also different from paradigms requiring learning and memory, regardless of whether it is direct or indirect learning. Our findings suggest that a generator in medial PF cortex maybe involved in the executive control of sensory information which links early gating in and gating out phenomenon.

#### 4.2 Dynamics of the M50 network

The estimated morphology of the neuromagnetic responses produced by the cortical sources underlying the M50 network indicated the existence of two middle latency cortical subcomponents, Mb1c and Mb2c, elicited by both tones of the oddball paradigm. These results agree with a previous study, reporting an early auditory evoked response composed of two subcomponents peaking at approximately 52 ms and 74 ms (Yvert et al., 2001). In particular, responses of both STG sources were found to be composed of two consecutive cortical subcomponents, Mb1c peaking at 35–53 ms and Mb2c peaking at 75–99 ms post-stimulus, without a significant difference in latencies across tone conditions. The estimated cortical response elicited by the PF source has an analogous tandem form, but significantly shorter latencies for both subcomponents evoked by the deviant tone. The observed difference in the latencies, but not in the strengths, of the PF source responses as a function of the tone condition may indicate a different type of modulation emerging from the same neuronal population in PF cortex related to gating in and gating out processing.

#### 4.3 Modulatory role of the PF generator

We found two types of task-activated auditory M50 networks which were differentiated by the presence or absence of the PF source in an age-homogeneous group of elderly subjects (>63 years). All nine subjects, lacking the frontal generator within the M50 network, were diagnosed as MCI or AD. Our results suggest that the PF region plays a modulatory role over auditory activity, based on the differential analyses indicating a functional association with the bilateral STG sources within the M50 network. The Mb2c subcomponent of the STG responses evoked by the standard stimuli showed significantly increased strength (110%) in subjects lacking the PF source, along with significantly increased strength of both M50 subcomponents (74% and 129% for, Mb1c and Mb2c, respectively) evoked by the deviant stimuli. Estimated dipole dynamics in numerical simulations (Fig. 4) and spatiotemporal modeling of empirical data (not shown), suggested that increased strength of STG activity in a network without a PF source is not related to the number of localized sources, but more likely is due to the modulating influence of a PF source.

Since previous studies of gating mechanisms mainly investigated cortical responses from the temporal regions only, it was assumed that larger amplitude M50 components of the STG responses, evoked by standard tones, reflect impaired inhibition of redundant auditory stimuli due to impaired functioning of sources in the primary auditory cortex. Our identification of a PF source during the M50 response in an oddball paradigm suggests that PF activity may be responsible for the habituation of the STG responses during oddball and gating paradigms. Our results indicate a clear relation between the activation of a PF source within the M50 network and the successful habituation of the STG responses to repetitive (standard) stimuli.

In conclusion, this study provides novel insights into the topology and neurodynamics of the M50 middle latency auditory network by offering an alternative interpretation aimed at resolving the current ambiguity associated with its neural generators and their functional roles. This non-invasive functional brain imaging study provides an important characterization of the PF source activity within the auditory M50 network during the 30–100 ms interval. Also, the two task-activated M50 network types, characterized by the presence/absence of a PF source, enabled a differential analysis of its impact on the auditory responses of the STG sources within the M50 network. Our results suggest a model where sustained activity of the PF source in healthy elders exerts an inhibitory effect on the sensory STG sources. This inhibitory influence is compromised in mild MCI and AD. However, we acknowledge that the putative “modulatory” role of the PF source on STG activity remains speculative until further research, with larger sample sizes, can demonstrate a causal relationship.

## Acknowledgments

This work was supported by NIH grants R01 AG029495 and R01 AG020302. The content is solely the responsibility of the authors and does not necessarily represent the official views of the National Institutes on Aging or the National Institutes of Health. This work was also supported in part by a VA Merit Review grant, by the Department of Energy under Award Number DE-FG02-99ER62764 to the Mind Research Network, the Radiology Department at UNM SOM, the Research Service at the New Mexico VA Health Care System, The Mind Research Network (NIH grants from the National Center for Research Resources (5P20RR021938) and the National Institute of General Medical Sciences (8P20GM103472)), bilateral agreement between the University of New Mexico and University of Zagreb, and the Croatian Ministry of Science, Education, and Sport (grant 199-1081870-1252).

## References

- Adler LE, Pachtman E, Franks RD, Pecevich MC, Waldo M, Freedman R. Neurophysiological evidence for a defect in neuronal mechanisms involved in sensory gating in schizophrenia. *Biol Psychiat*. 1982; 17:639–655. [PubMed: 7104417]
- Ahlfors SP, Han J, Lin FH, Witzel T, Belliveau JW, Hämäläinen MS, Halgren E. Cancellation of EEG and MEG signals generated by extended and distributed sources. *Hum Brain Mapp*. 2010; 31:140–149. [PubMed: 19639553]
- Aine CJ, Huang M, Stephen J, Christner R. Multistart algorithms for MEG empirical data analysis reliably characterize locations and time courses of multiple sources. *NeuroImage*. 2000; 12:159–172. [PubMed: 10913322]
- Aine CJ, Adair J, Knoefel D, Hudson C, Qualls S, Kovacevic S, Woodruff C, Cobb W, Padilla D, Lee R, Stephen JM. Temporal dynamics of age-related differences in auditory incidental verbal learning. *Cogn Brain Res*. 2005; 24:1–18.

- Aine CJ, Chad C, Woodruff C, Knoefel JE, Adair JC, Hudson D, Qualls C, Bocholt J, Best E, Kovacevic S, Cobb W, Padilla D, Hart B, Stephen JM. Aging: compensation or maturation? *NeuroImage*. 2006; 32:1891–1904. [PubMed: 16797187]
- Aine CJ, Bryant JE, Knoefel JE, Adair JC, Hart B, Donahue C, Montano R, Hayek R, Qualls C, Ranken D, Stephen JM. Different strategies for auditory word recognition in healthy versus normal aging. *NeuroImage*. 2010; 49:3319–3330. 2010. [PubMed: 19962439]
- Aine CJ, Sanfratello L, Adair JC, Knoefel JE, Caprihan A, Stephen JM. Development and decline of memory functions in normal, pathological, and healthy successful aging. *Brain Topography*. 2011; 24(3-4):323–339. [PubMed: 21452018]
- Aine CJ, Sanfratello L, Ranken D, Best E, MacArthur JA, Wallace T, Gilliam K, Donahue CH, Montano R, Bryant JE, Scott A, Stephen JM. MEG-SIM: A web portal for testing MEG analysis methods using realistic simulated and empirical data. *Neuroinform*. 2012; 10:141–158.
- Aine CJ, Sanfratello L, Adair JC, Knoefel JE, Qualls C, Lundy SL, Caprihan A, Stone D, Stephen JM. Characterization of a Normal Control Group: Are they Healthy? *Neuroimage*. 2014; 84:796–809. [PubMed: 24060318]
- Barbas H, Ghashghaei H, Dombrowski SM, Rempel-Clower NL. Medial prefrontal cortices are unified by common connections with superior temporal cortices and distinguished by input from memory-related areas in the rhesus monkey. *J Comp Neurol*. 1999; 410:343–367. [PubMed: 10404405]
- Boutros NN, Torello MW, Barker BA, Tueting PA, Wu SC. The P50 evoked potential component and mismatch detection in normal volunteers: implications for the study of sensory gating. *Psychiat Res*. 1995; 57:83–88.
- Cabeza R, Anderson ND, Locantore JK, McIntosh AR. Aging gracefully: compensatory brain activity in high-performing older adults. *NeuroImage*. 2002; 17:1394–1402. [PubMed: 12414279]
- Cacace AT, Satya-Murti S, Wolpaw JR. Human middle-latency auditory evoked potentials: vertex and temporal components. *Electroenceph Clin Neurophysiol*. 1990; 77:6–18. [PubMed: 1688786]
- Cancelli I, Cadore IP, Merlino G, Valentinis L, Moratti U, Bergonzi P, Gigli GL, Valente M. Sensory gating deficit assessed by P50/Pb middle latency event related potential in Alzheimer's disease. *J Clin Neurophysiol*. 2006; 23:421–425. [PubMed: 17016152]
- Cavada C, Company T, Tejedor J, Cruz-Rizzolo RJ, Reinoso-Suarez F. The anatomical connections of the macaque monkey orbitofrontal cortex. *Cereb Cortex*. 2000; 10:220–10,242.
- Cheng CH, Pei-Ning W, Wan-Yu H, Yung-Yang L. Inadequate inhibition of redundant auditory inputs in Alzheimer's disease: An MEG study. *Biol Psychol*. 2012; 89:365–373. [PubMed: 22155475]
- Crosson PL, Johansen-Berg H, Timothy EJ, Behrens M, Robson D, Pinsk MA, Gross CG, Richter W, Richter MC, Kastner S, Rushworth MPS. Quantitative Investigation of Connections of the Prefrontal Cortex in the Human and Macaque using Probabilistic. *J Neurosci*. 2005; 25:8854–8866. [PubMed: 16192375]
- Dobbins IG, Schnyer DM, Verfaellie M, Schacter DL. Cortical activity reductions during repetition priming can result from rapid response learning. *Nature*. 2004; 428:316–319. [PubMed: 14990968]
- Edgar JC, Huang MX, Weisend MP, Sherwood A, Miller GA, Adler LE, Canive JM. Interpreting abnormality: an EEG and MEG study of P50 and the auditory paired-stimulus paradigm. *Biol Psychol*. 2003; 65:1–20. [PubMed: 14638286]
- Ermütlu MN, Demiralp T, Karamursel S. The effects of interstimulus interval on sensory gating and on preattentive auditory memory in the oddball paradigm. Can magnitude of the sensory gating affect preattentive auditory comparison process? *Neurosci Lett*. 2007; 412:1–5. [PubMed: 17197084]
- Freedman R, Adler LE, Myles-Worsley M, Nagamoto HT, Miller C, Kisley M, McRae K, Cawthra E, Waldo M. Inhibitory gating of an evoked response to repeated auditory stimuli in schizophrenic and normal subjects. Human recordings, computer simulation, and an animal model. *Arch Gen Psychiatry*. 1996; 53:1114–1121. [PubMed: 8956677]
- Garcia-Rill E, Skinner RD, Clothire J, Dornhoffer J, Uc E, Fann A, Mamiya N. The sleep state-dependent midlatency auditory evoked P50 potential in various disorders. *Thal Rel Syst*. 2002; 2:9–19.
- Garcia-Rill E, Moran K, Garcia J, Findley WM, Walton K, Strotman B, Llinas RR. Magnetic sources of the M50 response are localized to frontal cortex. *Clin Neurophysiol*. 2008; 119:388–398. [PubMed: 18078782]

- Golob EJ, Ringman JM, Irimajiri R, Bright S, Schaffer B, Medina LD. A StarrCortical event-related potentials in preclinical familial Alzheimer disease. *Neurology*. 2009; 73:1649–1655. [PubMed: 19917987]
- Grunwald T, Boutros NN, Pezer N, von Oertzen J, Fernandez G, Schaller C, Elger CE. Neuronal substrates of sensory gating within the human brain. *Biol Psychiatry*. 2003; 53:511–519. [PubMed: 12644356]
- Hillebrand A, Barnes GR. A quantitative assessment of sensitivity of whole head MEG to activity in the adult human cortex. *Neuroimage*. 2002; 16:638–650. [PubMed: 12169249]
- Huang M, Aine CJ, Supek S, Best E, Ranken D, Flynn ER. Multi-start downhill simplex method for spatio-temporal source localization in magnetoencephalography. *Electroenceph Clin Neurophysiol*. 1998; 108:32–44. [PubMed: 9474060]
- Huang MX, Edgar JC, Thoma RJ, Hanlon FM, Moses SN, Lee RR, Paulson KM, Weisend MP, Irwin JG, Bustillo JR, Adler LE, Miller GA, Canive JM. Predicting EEG responses using MEG sources in superior temporal gyrus reveals source asynchrony in patients with schizophrenia. *Clin Neurophysiol*. 2003; 114:835–850. [PubMed: 12738429]
- Huotilainen M, Winkler I, Alho K, Escera C, Virtanen J, Ilmoniemi RJ, Jaaskelainen IP, Pekkonen E, Naatanen R. Combined mapping of human auditory EEG and MEG responses. *Electroenceph Clin Neurophysiol*. 1998; 108:370–379. [PubMed: 9714379]
- Jessen F, Kucharski C, Fries T, Papassotiropoulos A, Hoenig K, Maier W, Heun R. Sensory gating deficit expressed by a disturbed suppression of the P50 event-related potential in patients with Alzheimer's disease. *Am J Psychiatry*. 2001; 158:1319–1321. [PubMed: 11481170]
- Josef Golubic S, Susac A, Grilj V, Ranken D, Huonker R, Haueisen J, Supek S. Size matters: MEG empirical and simulation study on source localization of the earliest visual activity in the occipital cortex. *Med Biol Eng Comput*. 2011; 49:545–554. [PubMed: 21476049]
- Kringelbach ML. The orbitofrontal cortex: linking reward to hedonic experience. *Nat Rev Neurosci*. 2005; 6:691–702. [PubMed: 16136173]
- Knight RT, Scabini D, Woods DL. Prefrontal cortex gating of auditory transmission in humans. *Brain Res*. 1989; 504:338–342. [PubMed: 2598034]
- Korzyukova O, Pflieger ME, Wagner M, Bowyer SM, Rosburg T, Sundaresana K, Elger CE, Boutros NN. Generators of the intracranial P50 response in auditory sensory gating. *Neuroimage*. 2007; 35:814–826. [PubMed: 17293126]
- Kovacevic S, Qualls C, Adair JC, Hudson D, Woodruff CC, Knoefel J, Lee RR, Stephen JM, Aine CJ. Age-related effects on superior temporal gyrus activity during an auditory oddball task. *Neuroreport*. 2005; 16:1075–1079. [PubMed: 15973151]
- Leahy RM, Mosher JC, Spencer ME, Huang MX, Lewine JD. A study of dipole localization accuracy for MEG and EEG using a human skull phantom. *Electroenceph Clin Neurophysiol*. 1998; 107:159–173. [PubMed: 9751287]
- Lerch JP, Pruessner J, Zijdenbos AP, Collins DL, Teipel SJ, Hampel H, Evans AC. Automated cortical thickness measurements from MRI can accurately separate Alzheimer's patients from normal elderly controls. *Neurobiol Aging*. 2008; 29:23–30. [PubMed: 17097767]
- Liégeois-Chauvel C, Musolino A, Badier JM, Marquis P, Chauvel P. Evoked potentials recorded from the auditory cortex in man: evaluation and topography of the middle latency components. *Electroenceph Clin Neurophysiol*. 1994; 92:204–214. [PubMed: 7514990]
- Logan JM, Sanders AL, Snyder AZ, Morris JC, Buckner RL. Under-recruitment and nonselective recruitment: dissociable neural mechanisms associated with aging. *Neuron*. 2002; 33:827–840. [PubMed: 11879658]
- Lu BY, Edgar JC, Jones AP, Smith AK, Huang MX, Miller GA, Canive JM. Improved test-retest reliability of 50 ms paired-click auditory gating using magnetoencephalography source modeling. *Psychophysiology*. 2007; 44:86–90. [PubMed: 17241143]
- Medvick, PA.; Lewis, PS.; Aine, C.; Flynn, ER. Monte Carlo analysis of localization errors in magnetoencephalography. In: Williamson, SJ.; Hoke, M.; Kotani, M.; Stroink, G., editors. *Advances in Biomagnetism*. New York: Plenum Press; 1989. p. 543-546.
- Mosher JC, Lewis PS, Leahy RM. Multiple dipole modeling and localization from spatiotemporal MEG data. *IEEE Trans Biomed Eng*. 1992; 39:541–557. [PubMed: 1601435]

- Price JL, Davis PB, Morris JC, White DL. The distribution of tangles, plaques and related immunohistochemical markers in healthy aging and Alzheimer's disease. *Neurobiol Aging*. 1991; 12:295–312. [PubMed: 1961359]
- Ranken, DM.; Best, ED.; Stephen, JM.; Schmidt, DM.; George, JS.; Wood, CC.; Huang, M. MEG/EEG forward and inverse modeling using MRVIEW. Proceedings of the 13th international conference on biomagnetism; VDE Verlag; Berlin. 2002. p. 785-787.
- Ranken DM, Stephen JM, George JS. MUSIC Seeded Multi-Dipole MEG Modeling Using the Constrained Start Spatio-Temporal Modeling Procedure. *Neurol Clin Neurophysiol*. 2004; 2004:80. [PubMed: 16012631]
- Reite M, Teale P, Zimmerman J, Davis K, Whalen J. Source location of a 50 msec latency auditory evoked field component. *Electroencephalogr Clin Neurophysiol*. 1988; 70:490–498. [PubMed: 2461283]
- Rule RR, Shimamura AP, Knight RT. Orbitofrontal cortex and dynamic filtering of emotional stimuli. *Cogn Affect Behav Ne*. 2002; 2:264–270.
- Sanfratello, L.; Stephen, J.; Best, E.; Ranken, D.; Aine, CJ. MEG-SIM Web Portal: A database of realistic simulated and empirical MEG data for testing algorithms. In: Supek S, S.; Aine, CJ., editors. *Magnetoencephalography: From Signals to Dynamic Cortical Networks Heidelberg*. Springer Verlag; 2014. (in press)
- Shimamura AP. "The role of the prefrontal cortex in dynamic filtering" (PDF). *Psychobiology*. 2000; 28:207–218.
- Stephen JM, Ranken D, Best E, Adair J, Knoefel J, Kovacevic S, Padilla D, Hart B, Aine C. Aging changes and gender differences in response to median nerve stimulation measured with MEG. *Clin Neurophysiol*. 2006; 117:131–143. [PubMed: 16316782]
- Supek S, Aine CJ. Simulation studies of multiple dipole neuromagnetic source localization: Model order and limits of source resolution. *IEEE Trans Biomed Eng*. 1993; 40:529–540. [PubMed: 8262534]
- Supek S, Aine CJ. Spatio-temporal modelling of neuromagnetic data: Multi -source location versus time-course accuracy. *Hum Brain Map*. 1997; 5:139–153.
- Teo C, Rasco L, Al-Mefty K, Skinner RD, Boop FA, Garcia-Rill E. Decreased habituation of midlatency auditory evoked responses in parkinson's disease. *Mov Disord*. 1997; 12:655–664. [PubMed: 9380045]
- Thoma RJ, Hanlon FM, Moses SN, Edgar JC, Huang M, Weisend MP, Irwin J, Sherwood A, Paulson K, Bustillo J, Adler LE, Miller GA, Canive JM. Lateralization of auditory sensory gating and neuropsychological dysfunction in schizophrenia. *Am J Psychiatry*. 2003; 160:1595–1605. [PubMed: 12944333]
- Thomas C, VomBerg I, Rupp A, Seidl U, Schröder J, Roesch-Ely D. P50 gating deficit in Alzheimer dementia correlates to frontal neuropsychological function. *Neurobiol Aging*. 2010; 31:416–424. [PubMed: 18562045]
- Uc EY, Skinner RD, Rodnitzky RL, Garcia-Rill E. The midlatency auditory evoked potential P50 is abnormal in Huntington's disease. *J Neurolog Sci*. 2003; 212:1–5.
- Wan L, Friedman BH, Boutros NN, Crawford HJ. P50 sensory gating and attentional performance. *Int J Psychophysiol*. 2008; 67:91–100. [PubMed: 18036692]
- Weiland BJ, Boutros NN, Moran JM, Tepley N, Bowyer SM. Evidence for a frontal cortex role in both auditory and somatosensory habituation: a MEG study. *Neuroimage*. 2008; 42:827–835. [PubMed: 18602839]
- Woods DL, Knight RT, Neville HJ. Bitemporal lesions dissociate auditory evoked potentials and perception. *Electroenceph Clin Neurophysiol*. 1984; 57:208–57,220.
- Yvert B, Crouzeix A, Bertrand O, Seither-Preisler A, Pantev C. Multiple supratemporal sources of magnetic and electric auditory evoked middle latency components in humans. *Cereb Cortex*. 2001; 11:411–423. [PubMed: 11313293]

### Highlights

- Three cortical regions, bilateral STG and PF, identified as M50 complex generators.
- Sustained activity of PF source demonstrated inhibitory effects on the STG sources
- Significantly enhanced STG activity found for all subjects lacking a PF source.
- Simulations confirmed detectability of even very weak PF sources in the M50 network.

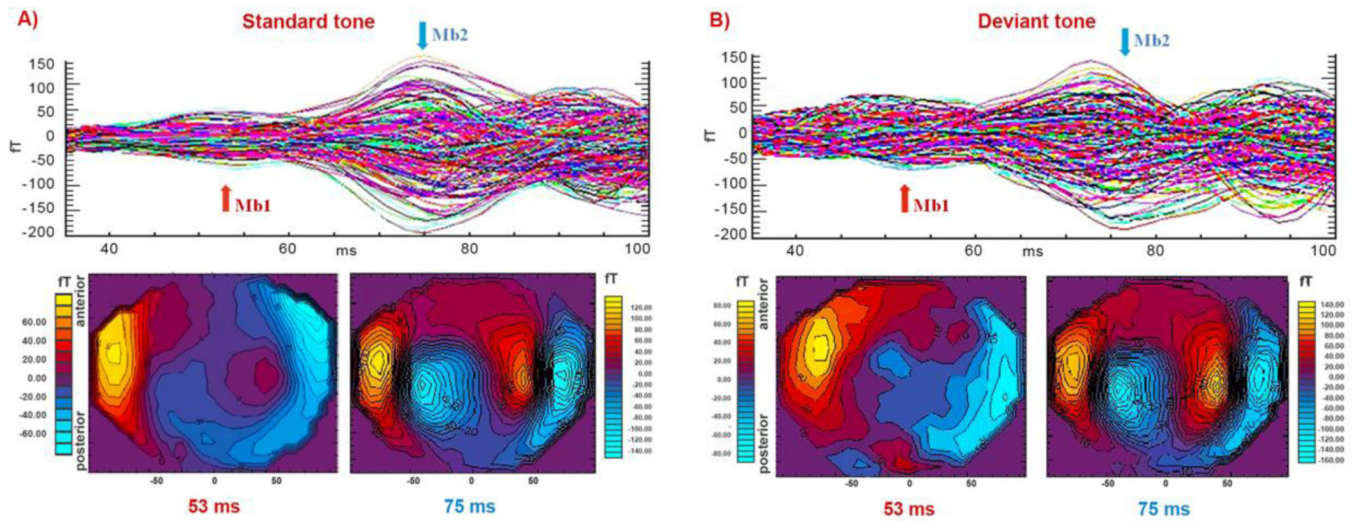


**Fig. 1.**

Auditory evoked neuromagnetic responses across the gradiometer channels (five noisy occipital channels are not included) for the standard (panel A) and the deviant tone (panel B) conditions, respectively, for representative subject (S1). Each tracing represents an average of 400 (standard tones) or 100 (deviant tones) individual neural responses. Iso-field color-coded maps of the AEFs obtained from all magnetometers are shown below the measured AEF waveforms. Black iso-field lines are shown at 20 fT levels. Magnitudes of positive fields (flux emerging from the head) are displayed in shades of yellow-red while negative fields are shown in shades of blue. Scale values, different for each map, are indicated at the left or right of the maps. The arrows above the waveforms indicate the peak latencies Mb1 and Mb2 for which the iso-field maps are displayed. Both data representations reveal two prominent peaks of the evoked activity during the 30–100 ms time interval.

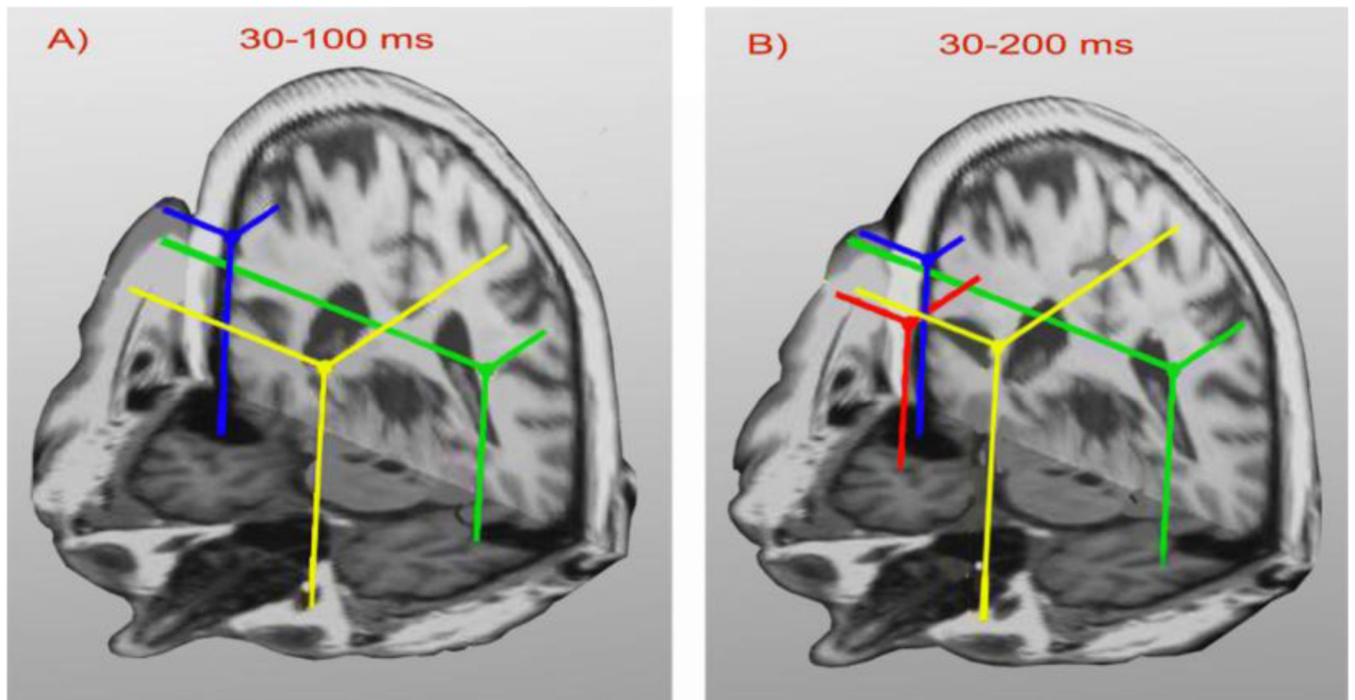


**Fig. 2.** Ten best fitting source locations for each cortical location (bilateral STG and PF), obtained for 30–100 ms (panel A) and 30–200 ms (panel B) time windows, for the same subject are shown in an anterior axial-coronal 3-D view. Bilateral STG sources (green and blue dots) and a PF source (yellow dot) are evident in both the 3- and 4-dipole solutions across time intervals. An additional source (red) was evident in the 30–200 ms interval.

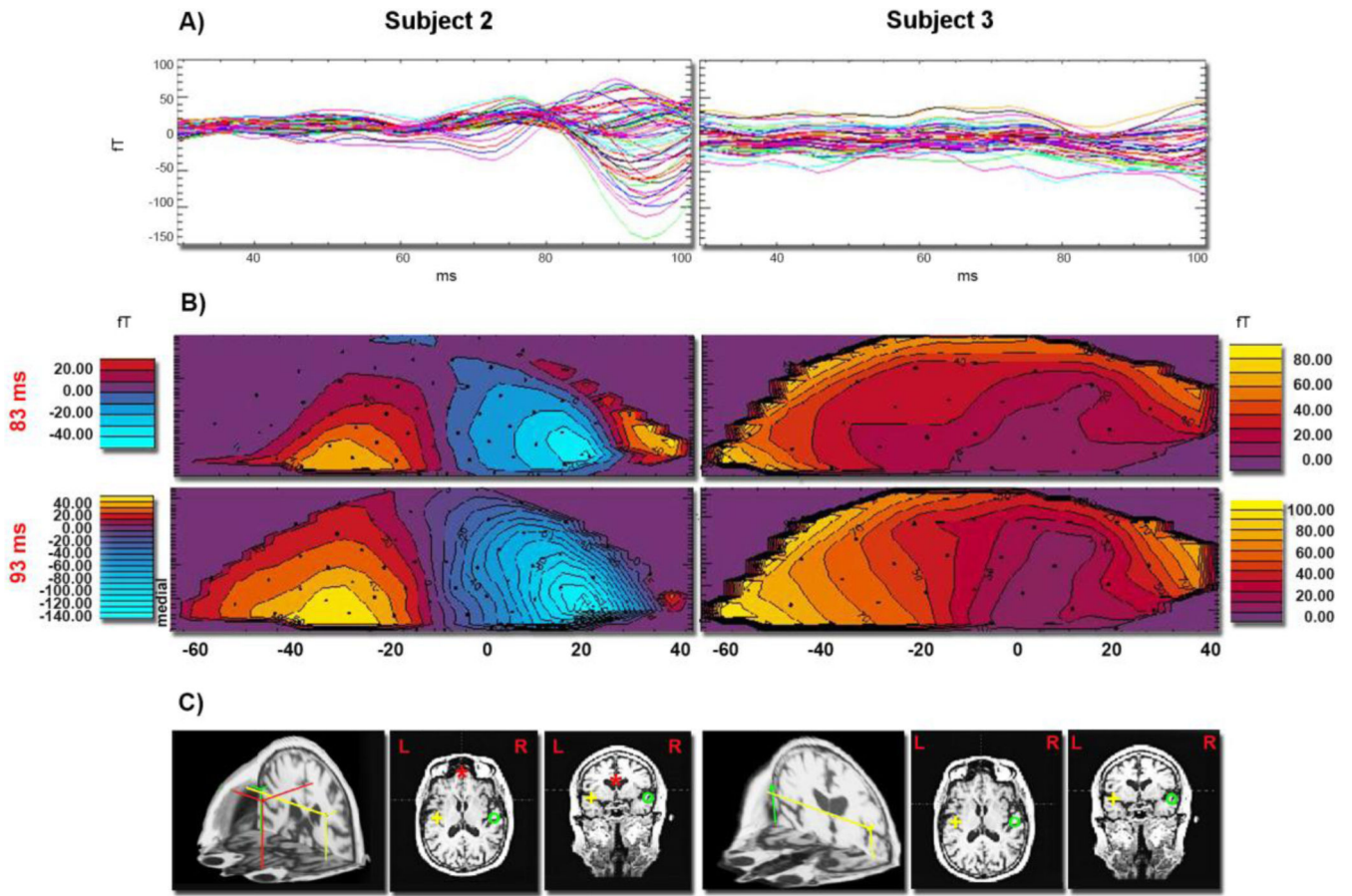


**Fig. 3.**

A) AEFs from the standard tone are shown superimposed from the frontal MEG channels (from MLF11 to MLF64) during the 30–100 ms time interval for two representative subjects, S2 and S3. Each tracing represents an average of 400 individual evoked responses. AEF waveforms obtained from the frontal sensors of subject S2 have a characteristic multi-peak pattern in contrast to the waveforms obtained from the same sensors of subject S3. Panel B) shows iso-field color-coded maps of the neuromagnetic responses recorded at frontal gradiometers evoked by the standard tone at two time points showing the Mb2 component of the M50 complex (around 85 ms), for two subjects. Black dots indicate sensor positions. The formation of a dipolar pattern in frontal regions of subject S2 is clearly missing in the corresponding iso-field maps of subject S3. Fragments of right STG activity are also visible in the field maps of subject S2. In panel C) the best fitting sources estimated in the 30–100 ms time interval evoked by the standard tone are shown for subjects S2 and S3 in 3-D and horizontal and coronal 2-D views. While both subjects revealed activation of bilateral STG generators, the frontal source localized in subject S2 was lacking in subject S3.

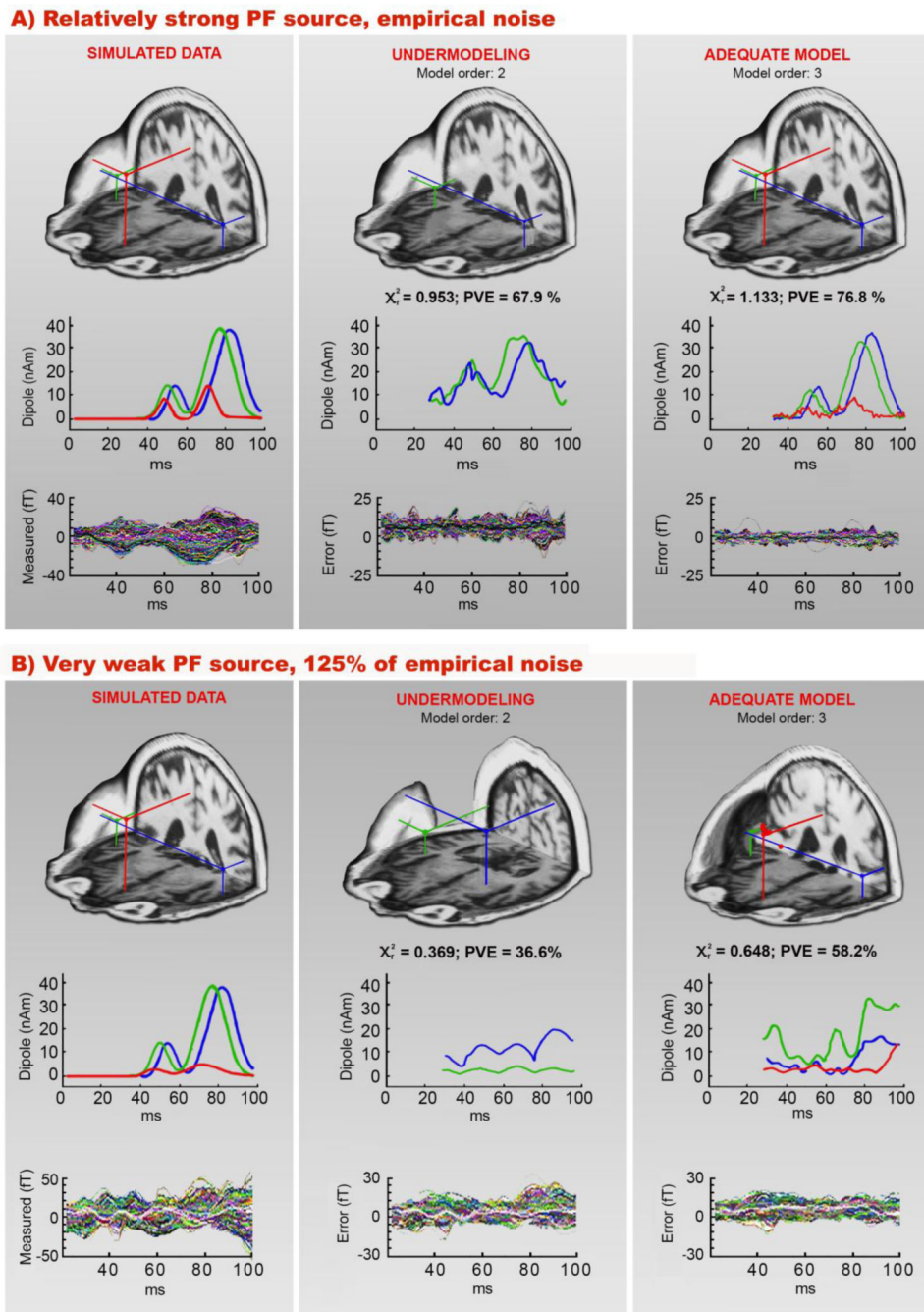


**Fig. 4.** Numerical simulations showing the two extreme cases of PF source strengths. Simulated source configuration and modeling results are shown for M50 networks where PF activity was varied from being a relatively strong source (panel A) to a very weak source (panel B). The left column of (A) and (B) shows simulated source locations, along with their time courses, and their corresponding noisy simulated waveforms; empirical activity obtained from the pre-stimulus interval ( $-100 - 0$  ms) was added to the waveforms (100% in panel A and 125% in panel B). Two strong bilateral sources were placed in the vicinity of the STG

on the realistic cortical surface of subject S2 (at a depth of 0.9 cm) and the PF source was placed in the medial region of the frontal lobe at a depth of 3.24 cm. Modeling results assuming 2- and 3-dipole models (ten best-fitting location and time course estimates) and the residual (“error”) waveforms from all channels, are shown in the middle and the right columns. The extreme noise level and attenuation of PF source strength influenced the estimated time courses more than their spatial localization (right column of panel B).

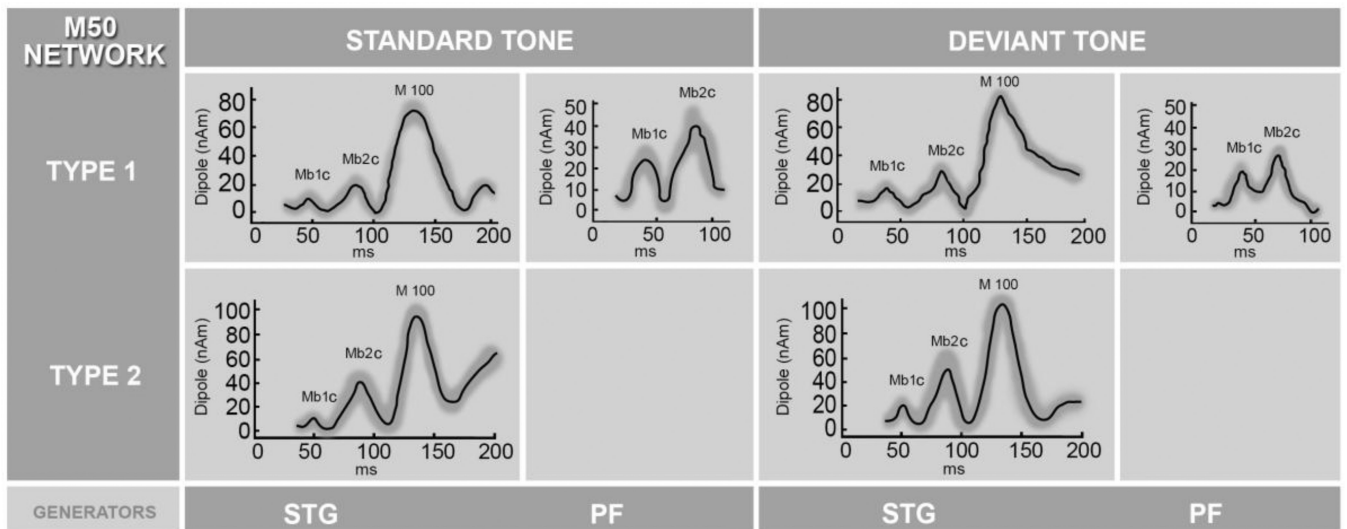


**Fig. 5.**

Estimated time courses of PF and STG sources underlying the M50 complex formation averaged across all subjects for the standard and deviant tones. In the elderly controls (network type 1) three generators of the M50 network were identified, bilateral STG and the PF source. In contrast, MCI/AD subjects (network type 2) showed no frontal activity. Time courses of the STG activity were averaged across subjects and hemispheres (standard deviations shown as a gray band), and displayed for the 30–200 ms time window to include M100, the most prominent STG response. The M100 is used for amplitude comparison with earlier cortical Mb1c and Mb2c components.

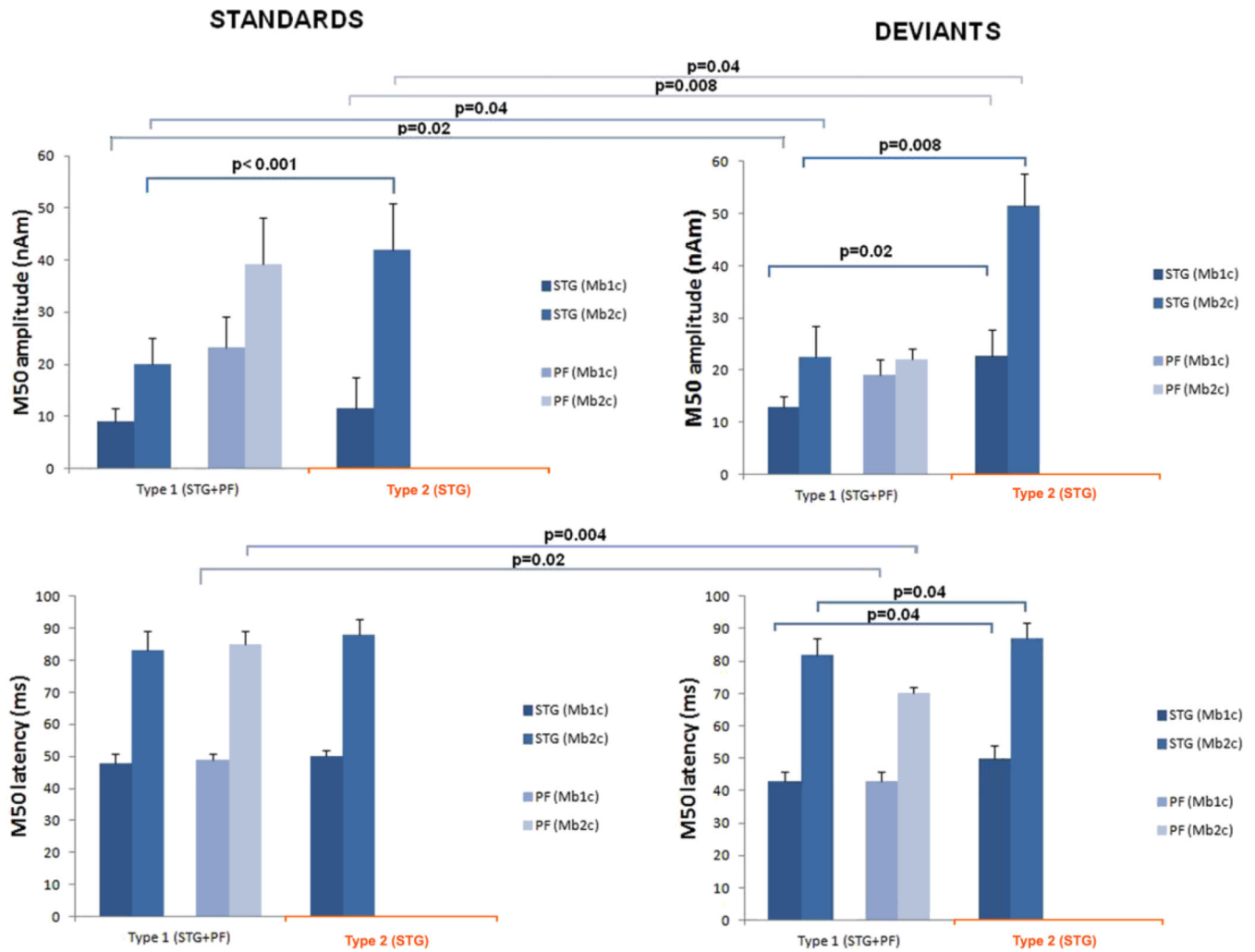


**Fig. 6.** Histograms showing the mean peak (cortical Mb1c and Mb2c) amplitudes and latencies of the estimated cortical dynamics of the sources underlying M50 complex across conditions (standard and deviant) and network types (STG+PF vs. STG only). The bar above each column indicates the standard deviation of the mean. Statistically significant differences are indicated with p-values.

**Table 1**

Simulations		Localization error (cm)		
PF dipole strength	Empirical noise	PF	left STG	right STG
15 nAm	100 %	0.16	0.25	0.25
	125 %	0.18	0.37	0.37
10 nAm	100 %	0.23	0.23	0.23
	125 %	0.34	0.35	0.34
7 nAm	100 %	0.42	0.23	0.23
	125 %	0.65	0.35	0.35
5 nAm	100 %	0.68	0.23	0.23
	125 %	0.82	0.35	0.35